Wire mesh sensor measurements of a co-current two-phase flow in a spent fuel pool-like rack

G Brillant, Benjamin Fourré

WIRE MESH SENSOR MEASUREMENTS OF A CO-CURRENT TWO-PHASE FLOW IN A SPENT FUEL POOL-LIKE RACK

G. Brillant and B. Fourré
PSN-RES/SEREX, IRSN, France
(Email: Guillaume.brillant@irsn.fr, Benjamin.fourre@irsn.fr)

ABSTRACT

Increased attention has been paid in the last decade to the Spent Fuel Pools (SFP) accident phenomenology. The DENOPI project conducted by the IRSN is part of this approach with the aim to gain knowledge in the SFP under loss of cooling or loss of coolant accident conditions and to better evaluate the safety margins. Questions are still pending regarding the issues of convective heat transfer under natural circulation due to a loss of cooling. For instance, the validation of computer codes for accident analysis in case of a natural circulation flow in a fuel assembly with boiling at atmospheric pressure requires additional experimental data. In that view, the MEDEA facility has been set up to study, *inter alia*, a co-current air/water flow in a SFP-like rack with a one meter height rod bundle. The pressure loss and void fraction are measured all along the fuel bundle using several pressure transducers. Besides, the void fraction and the bubble distribution at the outlet of the pool rack are obtained by means of a Wire Mesh Sensor (WMS).

KEYWORDS
LOSS-OF-COOLING/COOLANT ACCIDENT, SPENT FUEL POOL, TWO PHASE FLOW, WIRE MESH SENSOR

1. INTRODUCTION

Since the Fukushima-Daiichi accident, much attention has been paid to the vulnerability of Spent Fuel Pools (SFP) [1–4]. Numerous countries and institutions have initiated a deep assessment of the safety of their operated SFP and have pursued or launched research activities in SFP [5-10]. In this context, the DENOPI project [11–13] has been launched by the IRSN (the French Technical and Scientific Support Organization) in collaboration with several research laboratories with the aim of studying the behavior of spent fuel pools under Loss-of-Cooling and Loss-of-Coolant Accidents (SFP-LOCA). The DENOPI project is a research program including both experimental and modeling activities. Its purpose is to provide code developers with an experimental database, made up of SFP integral and separate effect tests, for code improvement and validation. The project is divided into three axes, each corresponding to a specific spatial scale involved in a SFP-LOCA. The first axis is related to natural circulation occurring at the pool scale, prior to the fuel uncovery. The thermal-hydraulics of a typical PWR (Pressurized Water Reactor) fuel bundle prior to and after the fuel uncovery is investigated in the second axis. In particular, the efficiency of spray cooling systems as a mitigation measure is assessed. Finally, the third axis is dedicated to the fuel cladding degradation by steam-air mixture oxidation after fuel uncovery.

Within the framework of the DENOPI project, and more specifically in its second axis, the IRSN built the MEDEA mock-up. The main component of this facility is a one meter high unheated rod bundle. The objective of this experimental set-up is to get new insights on the physical phenomena involved during uncovering and water spraying of a fuel bundle stored in a spent fuel pool. The MEDEA program has two main steps. The first one is focused on air/water experiments, and the second one on steam/water experiments. The air/water experiments are of two kinds: the study of flooding in case of water spraying on a completely uncovered bundle (MEDEA-flooding tests) and the study of the void distribution along a fully covered assembly in an air/water co-current flow (MEDEA-overflow tests). The results of the MEDEA-overflow tests are presented in this article.

In 2015, a working group set up at OECD/NEA issued a status report on SFP Loss-of-Cooling and Loss-of-Coolant Accident (SFP-LOCA), that aims at providing a summary of the status of SFP accident and mitigation strategies, a brief review of the state of the art of the simulation tools potentialities for SFP-LOCA assessment and a proposal for some additional research actions [14]. Moreover, a European NUGENIA project named Air-SFP was performed in 2015-2016, in order to assess the uncertainties of Severe Accident (SA) codes in dealing with SFP-LOCA and to identify needs of modeling improvement [15]. Recently, a Phenomena Identification Ranking Table (PIRT) activity related to SFP-LOCA was carried out at OECD/NEA [16]. From these activities, it appears that the validation database of most computer codes currently used for SFP deterministic safety analysis (system codes developed on the basis of in-reactor incidental or accidental conditions) need to be extended to SFP configurations. Indeed, the thermal-hydraulics of a SFP is mainly based on natural convection flows (gaseous, liquid or two-phase flows), developed at atmospheric pressure with a relatively low heat load, compared to in-reactor conditions. These current codes haven't been primarily developed for natural convection flows and their applicability to SFP has to be improved. The MEDEA-overflow tests aim at studying the pressure loss and void fraction along a PWR fuel bundle for a co-current air/water flow at room temperature and atmospheric pressure. These measurements are required for the validation of thermal-hydraulics numerical tools, especially regarding the drift flux models for the low pressure domain of natural flow in a fuel bundle. This air/water flow study is a first approach to observe and measure the flow pattern and void fraction for a co-current gas/liquid flow awaiting the ASPIC facility. Actually, the ASPIC facility, currently under construction, is a full height 17x17 assembly with heated rods (80 kW, up to 600 °C) that will enable several kinds of experiments and scenarios for SFP accidents at the assembly scale.

This article is organized as follows. In section 2, a presentation of the MEDEA device and measurement apparatus is driven. The test protocol is laid out in section 3. Then, the results of the reference test are stated and analyzed in section 4. Finally, the main outcomes of this experimental study are drawn in the conclusion.

2. EXPERIMENTAL SET-UP

MEDEA is a thermalhydraulics facility of the IRSN platform THEMA (THErmalhydraulics for Mitigation of Accidents) which will also include in the near future ASPIC [11] and MIDI [12, 17]. The overflow configuration of the MEDEA facility is composed of a test section with a one meter high rod bundle, an air injection line connected to the bottom of the test section, a water injection line connected to the bottom of the test section, and a water gathering circuit for the overflow liquid (*Cf.* figure 1).

The central test section of MEDEA is a square tube with an internal dimension of 225 mm corresponding to a cell of a spent fuel pool rack. A 17x17 rod bundle is inserted inside the test section. This bundle has a reduced height of 1240 mm for a weight of about 80 kg. The top nozzle, spacer grids, and rods are representative to a typical PWR rod bundle. The free flow area of the top

nozzle is about 205 cm^2. Below the test section with the rod bundle, the lower section aims at injecting the water flow and the air bubbles and obtaining a stationary flow at the bottom of the rod bundle. The length of the lower section is 1416 mm (about 6 hydraulic diameters). Above the test section, the upper head is connected to the gathering water line that collects the overflow. About 317 mm below the overflow level a Wire Mesh Sensor (WMS) [18] is placed. This apparatus measures the void fraction on a grid pattern (96x96 wires with a 4 mm spacing). A WMS consists of several wire electrodes stretched in two adjacent planes and in perpendicular orientation across the flow cross-section. Electrodes in one plane act as electrical transmitters, whereas the ones in the other plane act as receivers. With a special excitation scheme, one can measure the electrical resistance/conductance in each crossing point of the sensor at high speed. Extended details on the WMS technique can be found in [19, 120].

The air injection line is equipped with a flowmeter/valve group (to regulate the air volume flowrate injected in the test section). The flowmeter/valve group is used in automatic mode (operator sets the target volume flowrate which is stabilized by means of a PID controller). The water injection line is connected to a tank with a capacity of 2000 l. The water is pumped from that tank and flows through a flowmeter/valve group. This group can either be used in manual or automatic mode to set up the water mass flowrate in injection line. The water flows through the central section and the rod bundle. Note that a bypass line can be partially opened with manual valve to send back part of the water flow directly to the main tank. The water flow above the rod bundle and the WMS leads to an overflow that is collected and sent back to the main tank by means of the water gathering line (gravity flow).

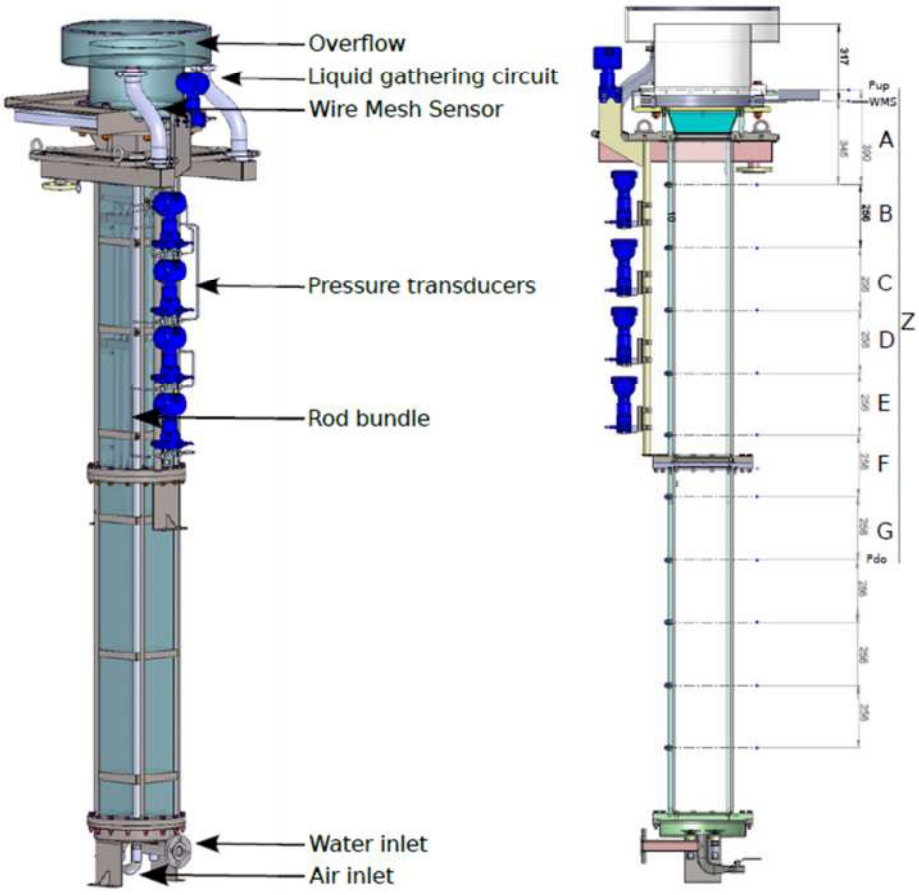

Figure 1: Test section of the MEDEA-overflow configuration and location of the pressure measuring holes.

3. TEST PROTOCOL AND PARAMETERS

The test series were carried out by varying the air flowrate at a given water flowrate. Actually, the series started with a test at zero air flowrate to determine the default signal of all the pressure transducers. That way, the transducers inherent offset (e.g. due to transducer orientation) as well as the potential dynamic pressure offset can be subtracted from the other tests with positive gas flowrates. Note that the free flow section is not constant along the test section which leads to variations of the water velocity and thus of the dynamic pressure. For each test, the signal of the pressure transducers is recorded over at least 10 min at 1 Hz. Hence, stabilized mean and standard deviation values of the pressures can be calculated. Note that the pressure transducers have a span of -20/20 mbar and a time response of 100 ms. Besides, five recording of 1 min at 400 Hz are performed with the WMS. From those measurements, the radial profile of the void fraction is estimated as well as the distribution of the bubble sizes on each recording and a mean curve is obtained over the five recordings. The locations of all the pressure transducers and the WMS are reported in figure 1. The uncertainties of the pressure measurements, considering both the sensor and the supply chain, are 0.05 mbar for the differential pressure transducers dP_A–dP_G and 1.5 mbar for the absolute pressure transducers P_{up} and P_{do}. Regarding the flowrate measurements, the uncertainties are 1% for the air flow and 0.1% for the water flow.

The parameters of the MEDEA-overflow test series are the water mass flowrate, the air volume flowrate and the geometrical configuration. Two configurations have been considered: with (configuration C1) and without (configuration C2) the rod bundle inside the central test section. That way, the impact of the rod bundle on the evolution of the pressure loss and void fraction along the test section can be evaluated. The range of the water mass flowrate is 400 g/s to 2400 g/s and the range of the air volume flowrate is 10 Nl/min to 180 Nl/min (flowrate at 0 °C and 1 atm). In the present article, the focus is put on the tests with a water flowrate of 1200 g/s with the fuel bundle inside the test section.

4. RESULTS

4.1 Zero air flow measurements

The pressures from all the transducers were recorded at zero air flow condition. From the absolute pressure transducers, it can be noticed a difference $dP_Z = P_{do} - P_{up}$ of 196.0 mbar at low water mass flowrates. The difference of elevation between the two transducers up and down can then be deduced to H = 2006 mm (with g = 9.807 m/s^2 and ρ = 966.1 kg/m^3). The pressure difference increases with the liquid mass flowrate up to 197.0 mbar while the standard deviation remains below 0.5 mbar. The free fluid section at P_{up} (resp. P_{do}) connection is about 11.8 dm^2 (resp. 5.06 dm^2). Hence, the dynamic pressure drop between these two sensors is lower than 0.01 mbar and can be neglected hereafter. Note that the 1 mbar observed in the range of the studied water mass flowrates is within the uncertainty of 1.5 mbar of the absolute pressure transducers. Considering the 264 rods with an external diameter of 9.52 mm and 25 guide tubes with an external diameter of 12 mm (12.45 mm in reactor), the free flow surface in the rod bundle (outside grids) is about 2.90 dm^2. The dynamic pressure drops for the transducers B, C, D, E, and G is almost zero since the free flow surface facing the connection holes is constant. For the other transducers (A and F) the maximum dynamic pressure drop can be estimated to 0.01 mbar. Actually, a maximum variation of about 0.23 mbar is noticed as the water flowrate increases from 400 g/s to 2400 g/s. Since the standard deviation of the pressure drop is about 0.05 mbar and the transducers accuracy is 0.05 mbar, the dynamic pressure drops for these differential pressure transducers can be neglected.

4.2 Pressure measurements for the reference test series

For the reference test series, the water mass flowrate is set to 1200 g/s and eleven values of the air volume flowrate are considered in the range 0 Nl/min to 180 Nl/min. The water mass flowrate is kept constant during each test (meaning each plateau of air volume flowrate). As the friction inside the test section evolves with the air volume flowrate, the opening rate of the valve on the water line was adapted on each test to stick to the target value of the water mass flowrate. In doing so, the mean value of the water mass flowrate is kept in the range 1198 g/s to 1223 g/s (2 % maximum deviation). It can be noticed that, for all tests, the standard deviation of the water mass flowrate is around 1.5 g/s.

The value of the mean and the standard deviation of the pressure difference $(P_{do} - P_{up})$ on the test section is given in figure 2. This pressure difference decreases from 196.0 mbar to 165.9 mbar while the air flowrate rises from 0 Nl/min to 180 Nl/min. Besides, it can be observed that the air volume flowrate has no clear impact on the standard deviation of the pressure difference. The pressure difference can be written as (terms with air density are neglected as well as the dynamic pressure drop between two sensors):

$$dP_Z = P_{do} - P_{up} = (1 - \alpha_Z) \cdot \rho_w \cdot g \cdot h + \rho_w \cdot g \cdot (H - h) \tag{1}$$

where H is the elevation difference between the two transducers, h the elevation difference between the two connection holes on the central section, and α_Z the mean void fraction along the test section between the two holes where the two transducers P_{up} and P_{do} are connected. Therefore, the void fraction α_Z can be estimated as:

$$\alpha_Z = \frac{(\rho_w \cdot g \cdot H - dP_Z)}{\rho_w \cdot g \cdot h} \tag{2}$$

The measurements from the differential pressure transducers are gathered in figure 3. The mean values range from 0 mbar to 6 mbar. On the contrary to the observation made on the absolute pressure measurements, the air volume flowrate has a clear impact on the standard deviation of the differential pressure signals. In fact, the standard deviation increases with the air volume flowrate. It can be noticed that the standard deviation above the rod bundle (curve A) is higher than the standard deviation in the assembly area, revealing a more perturbed flow in this region. The differential pressures can be expressed as:

$$dP_i - dP_i^0 = \rho_w \cdot g \cdot dh_i - (1 - \alpha_i) \cdot \rho_w \cdot g \cdot dh_i \quad ; \quad i = A, \dots, G \tag{3}$$

with dP_i^0 the offset signal of the differential pressure transducers and dh_i the elevation difference between the two connections of the dedicated transducer. Therefore, the void fraction can be calculated as:

$$\alpha_i = \frac{(dP_i - dP_i^0)}{\rho_w \cdot g \cdot dh_i} \quad ; \quad i = A, \dots, G \tag{4}$$

The void fractions, calculated by means of the pressure measurements, are plotted in figure 4. Firstly, the lower values of the void fraction are measured above the rod bundle (transducer A). In fact, these smaller values may be imputed to the higher section radius above the assembly with a recirculation zone of water with almost no air at the periphery. What is surprising is the stabilization at this location of the void fraction around 7 % for the air volume flowrates higher than 120 Nl/min. The highest values of the void fraction are measured just below the rod bundle (transducer F) and are due to a plug created by the lower plate below the assembly. Note that this plug grows, as well as the void fraction, as the air volume flowrate rises. Intermediary void fraction are observed all along the rod bundle (transducers B-E) as well as in the lower part of the test section (transducer G). The impact of the grids on the void fraction profiles can be hardly explained. In fact, the transducers B (with a support grid) and D (with a mixing grid) lead to similar void fraction profiles but a different behavior is noted for the transducer E (with a support grid). The void fraction in the lower part of the test section (without assembly, transducer G) is lower than the void fraction along the rod bundle. This observation can be imputed to the higher friction in the assembly (due to both rods and grids) that restrain the bubble rise and, in a lower extend, to the evolution of the air compressibility with the absolute pressure. The mean void fraction (α_Z) over the full height of the test section measured by the two absolute pressure transducers is among the other void fraction curves measured locally by all the differential pressure transducers.

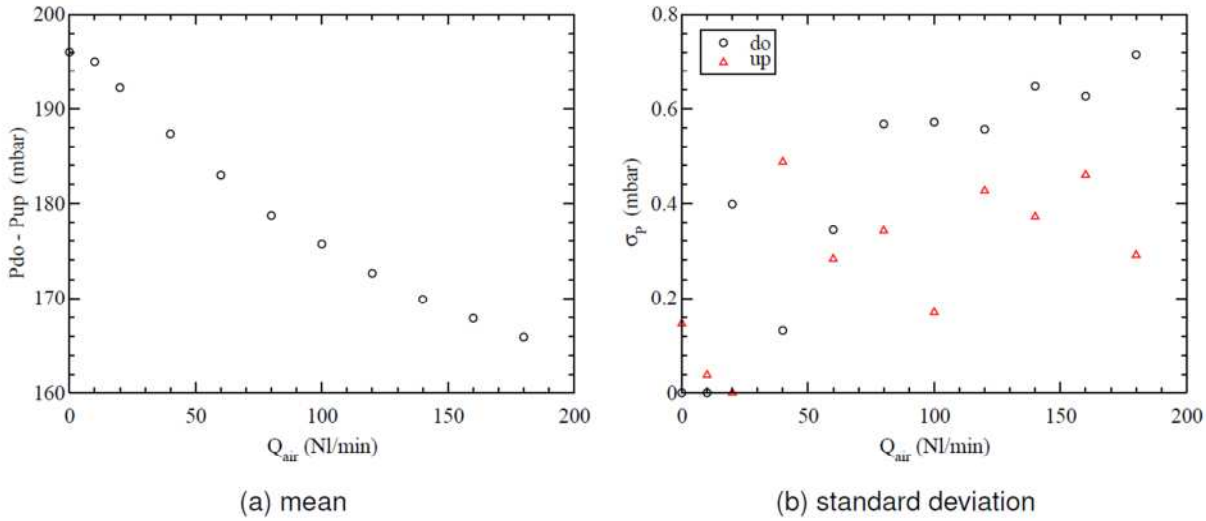

Figure 2: Pressure difference ($P_{do} - P_{up}$) for the tests at a water flowrate of 1200 g/s.

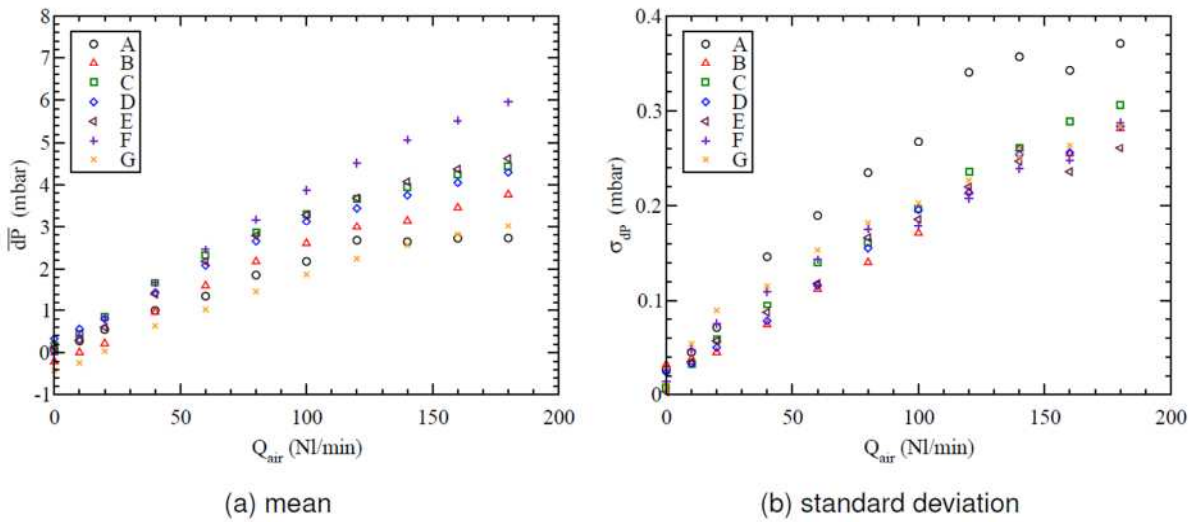

Figure 3: Differential pressure measurements for the tests at a water flowrate of 1200 g/s.

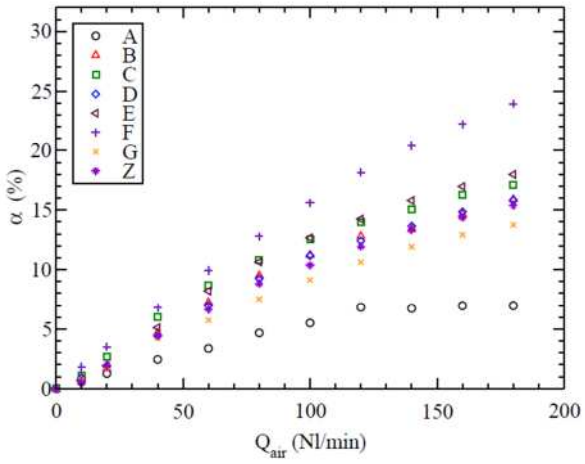

Figure 4: Void fraction for the tests at a water flowrate of 1200 g/s.

4.3 Wire mesh sensor measurements for the reference test series

Regarding the measurements with the WMS, five records of 1 min each have been made for all the air volume flowrate values. Figure 5a shows the five mean void fraction profiles over 1 min as long as the mean profile over these five former profiles (at the air volume flowrate of 100 Nl/min). Note that the circular section at the WMS elevation has a diameter of 388 mm. It can be observed that the void fraction profiles have always the same shape: the void fraction is maximum at the center of the test section and decreases towards the wall. Actually, at the section center, the void fraction varies in the range 8 % to 11 % with a mean value of 9.2 %.

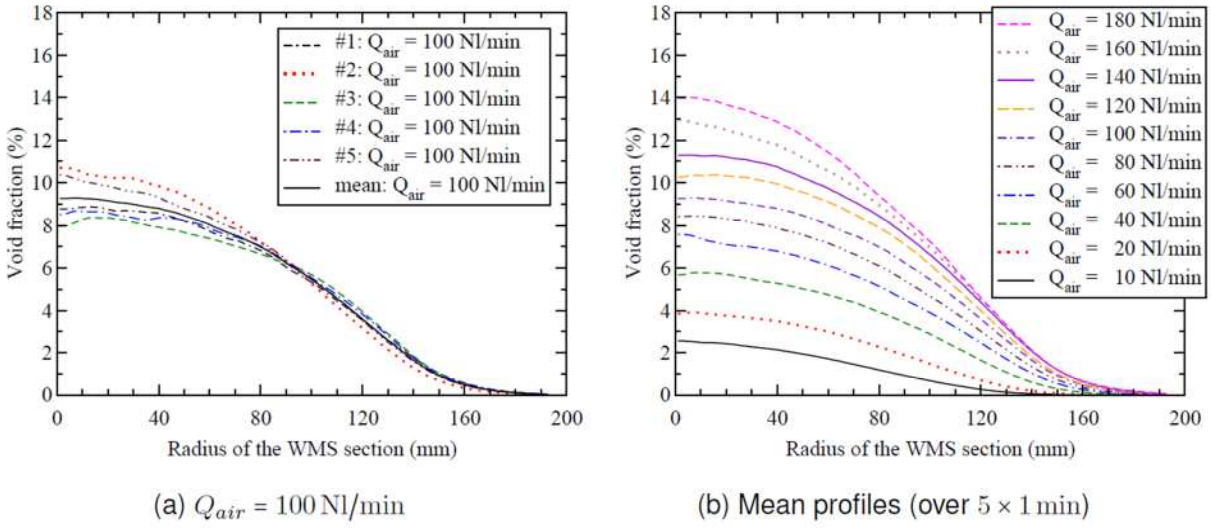

Figure 5: Void measurements with the WMS at Q_w = 1200 g/s.

The mean profiles are gathered in figure 5b for several air volume flowrates values. At the section center, the void fraction increases from 2 % to 14 % as the air volume flowrate varies from 10 Nl/min to 180 Nl/min. These values are smaller than the void fraction measured by means of the pressure transducers. Actually, it can be explained by the higher section radius at the WMS elevation. It can be noted that recirculations have been observed at the upper part of the central section. However, the mean void fraction from the WMS over a circle with a radius of 127 mm (corresponding to the section of the central section 225 mm × 225 mm) is quite similar to the void fraction measured by the upper pressure transducer A (Cf. figure 6). This points out the consistency of the measurements obtained by pressure transducers on one hand and by a WMS on the other hand. However, it can be noticed that the discrepancies on the void fraction estimations by the two sensors are higher than their respective uncertainties (about 10 % for the WMS [21] and 1 % for the pressure transducers). Actually the WMS is intrusive and the higher values of the void fraction from the WMS can be partially imputed to bubble entrapment at the grid. The bubble diameter histogram is reported in figure 7. It can be observed the overall enlargement of the bubble size with the air volume flowrate. Note that the histogram peak of the bubble diameter roughly evolves from 5 mm to 6 mm as the air flowrate increases.

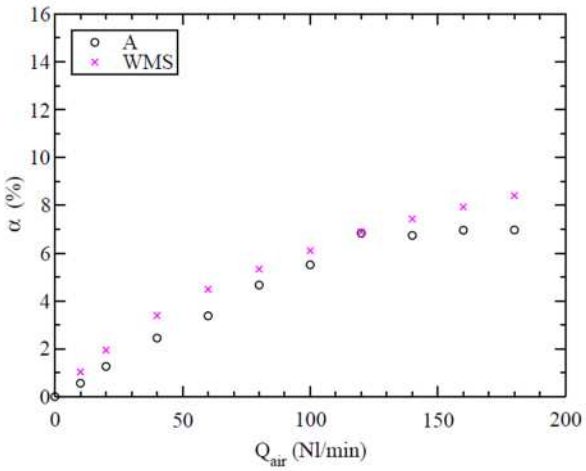

Figure 6: Comparison of the void fraction from transducer A and from WMS (mean value over a circle of radius 127 mm) at a water flowrate of 1200 g/s.

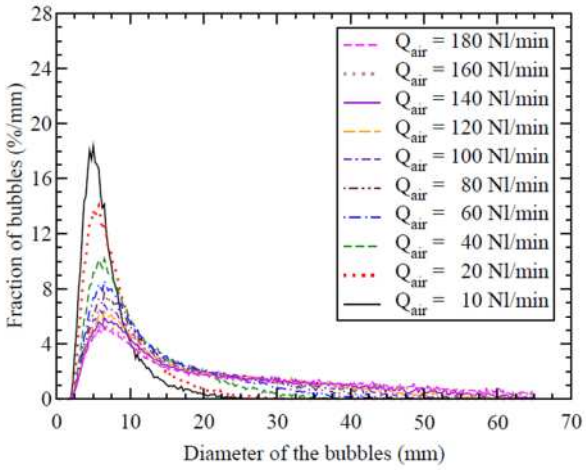

Figure 7: Bubble size distribution measured by the WMS for the tests at a water flowrate of 1200 g/s.

5. CONCLUSIONS

The results of the MEDEA-overflow experiments with a co-current air/water flow are presented in the present article. This experimental program aims at improving our understanding of the physical phenomena involved at the fuel assembly scale in a spent fuel pool in case of loss of cooling or loss of coolant accidents. In this contribution, the focus is put on the reference test series with a water mass flowrate of 1200 g/s. No clear impact of the mixing grids and support grids on the void fraction profiles could be evidenced. An asset of these experiments is the application of a WMS which leads to the measurements of the cross section void fraction profile as well as the bubble size distribution. It has been observed an enlargement of the bubbles as the air volume flowrate rises. Moreover, this study put in light the consistency of the measurements obtained by pressure transducers and by a WMS. Besides its intrinsic significance regarding the physical phenomena involved in a two-phase flow at a rod bundle scale, this experimental data can be directly considered to validate system codes such as DRACCAR [22] or ASTEC [23]. Actually, the flow simulation of a specific configuration by such numerical codes requires, *inter alia*, a correct estimation of the pressure drop and thus an appropriate drift flux model. This work will help to cover the gap of validation, especially for the drift flux model, for the low pressure domain in a PWR bundle geometry. To go further, higher water levels and heat transfer with steam instead of air are necessary. That will be possible in the near future thanks to the forthcoming ASPIC test rig which is a four meter height electrically heated rod bundle in a SFP rack. Beyond that, the ASPIC facility, will enable several kinds of experiments and scenarios for SFP accidents at the assembly scale.

6. ACKNOWLEDGEMENTS

The DENOPI project is part of the "Investment for the future" program funded by the French Government within the framework of the post-Fukushima surveys identified as major safety issues (contract number ANR 11 - RSNR 006). The authors are grateful to U. Hampel and E. Schleicher for their help on the use of the WMS.

7. REFERENCES

1. D. Wang, I.C. Gauld, G.L. Yoder, L.J. Ott, G.F. Flanagan, M.W. Francis, E.L. Popov, J.J. Carbajo, P.K. Jain, J.C. Wagner, and J.C. Gehin, "Study of Fukushima Daiichi nuclear power station unit 4 spent-fuel pool", *Nucl. Tech.*, **180**(2), pp. 205-215 (2012).
2. X. Wu, W. Li, Y. Zhang, W. Tian, G. Su, and S. Qiu, "Analysis of accidental loss of pool coolant due to leakage in a PWR SFP", *Ann. Nucl. Energy*, **77**, pp. 65-73 (2015).
3. Y.-S. Chen and Y.-R. Yuann, "Accident mitigation for spent fuel storage in the upper pool of a Mark III containment", *Ann. Nucl. Energy*, **91**, pp. 156-164 (2016).
4. J.H. Song and T.W. Kim, "Severe accident issues raised by the Fukushima accident and improvements suggested", *Nucl. Eng. Tech.*, **46**(2), pp. 207-216 (2014).
5. M. Arlit, C. Partmann, E. Schleicher, C. Schuster, A. Hurtado, and U. Hampel, "Instrumentation for experiments on a fuel element mock-up for the study of thermal hydraulics for loss of cooling or coolant scenarios in spent fuel pools", *Nucl. Eng. Des.*, **336**, pp. 105-111 (2018).
6. C. Partmann, C. Schuster, and A. Hurtado, "Experimental investigation of the thermal hydraulcs of a spent fuel pool under loss of active heat removal conditions", *Nucl. Eng. Des.*, **330**, pp. 480-487 (2018).
7. S.G. Durbin, E.R. Lindgren, A.S. Goldmann, M. Zavisca, Z. Yuan, R. Karimi, A. Krall, and M. Khatib-Rahbar, "Spent Fuel Pool Project phase I: Pre-ignition and ignition testing of a single commercial 17x17 pressurized water reactor spent fuel assembly under complete loss of coolant accident conditions", NUREG/CR-7215, U.S. Nuclear Regulatory Commission (2016).
8. S.G. Durbin, E.R. Lindgren, L. Humphries, Z. Yuan, M. Zavisca, M. Khatib-Rahbar, and R. Beaton, "Spent Fuel Pool Project phase II: Pre-ignition and ignition testing of a 1x4 commercial 17x17 pressurized water reactor spent fuel assemblies under complete loss of coolant accident conditions", NUREG/CR-7216, U.S. Nuclear Regulatory Commission (2016).
9. E.R. Lindgren and S.G. Durbin, "Characterization of thermal-hydraulic and ignition phenomena in prototypic, full-length boiling water reactor spent fuel pool assemblies after a postulated complete loss-of-coolant accident", NUREG/CR-7143, U.S. Nuclear Regulatory Commission (2013).
10. Z. Hózer, E. Szabó, T. Pintér, I. Baracska Varjú, T. Bujtás, G. Farkas, and N. Vajda, "Activity release from damaged fuel during the paks-2 cleaning tank incident in the spent fuel storage pool", *J. Nucl. Mater*, **392**(1), pp. 90-94 (2009).
11. H. Mutelle, I. Tamburini, C. Duriez, S. Tillard, N. Trégourès, A. Toutant, V. Mermoux, M. abd Peres, and H. Buscail, "A new research program on accidents in spent fuel pools: the DENOPI project", In WRFPM, Sensai, Japan, number 100071 (2014).
12. J. Martin, "Overview of the IRSN DENOPI project on spent fuel pool in loss-of-cooling and loss-of-coolant accident conditions", In CSARP, Bethesda, Maryland, USA (2016).
13. J. Martin, N. Trégourès, G. Brillant, C. Duriez, and C. Marquié, "The IRSN DENOPI project: a research program on spent-fuel-pool loss-of-cooling and loss-of-coolant accidents", In NURETH, Xi'an, China (2017).
14. "Status report on spent fuel pools under loss-of-cooling and loss-of-coolant accident conditions", NEA/OCDE 2015-2, Nuclear Energy Agency (2015).
15. O. Coindreau, B. Jäckel, F. Rocchi, F. Alcaro, D. Angelova, and G. Bandini, "Severe accident code-to-code comparison for two accident scenarios in a spent fuel pool", In The 8th European Review Meeting on Severe Accident Research - ERMSAR (2017).
16. "PIRT: R&D priorities for loss-of-cooling and loss-of-coolant accidents in spent nuclear fuel pools", NEA/OCDE 2017-18, Nuclear Energy Agency (2017).

17. N. Trégourès, “The DENOPI project: a research program on SFP under loss-of-cooling and loss-of-coolant accident conditions”, In IAEA, IE8M (2015).
18. H.-M. Prasser, A. Böttger, and J. Zschau, “A new electrode-mesh tomograph for gas-liquid flows”, *Flow Meas. Instrum.*, **9**(2), pp. 111-119 (1998).
19. Kipping R., R. Brito, E. Scheicher, and U. Hampel, “Developments for the application of the Wire-Mesh Sensor in industries”, *Int. J. Multiphase Flow*, **85**, pp. 86-95 (2016).
20. E. Schleicher, T.B. Aydin, R.E. Vieira, C.F. Torres, E. Pereyra, C. Sarica, and U. Hampel, “Refined reconstruction of liquid-gas interface structures for stratified two-phase flow using wire-mesh sensor”, *Flow Meas. Instrum.*, **46**, pp. 230-239 (2015).
21. C. Tompkins, H.-M. Prasser, and M. Corradini, “Wire-mesh sensors: A review of methods and uncertainty in multiphase flows relative to other measurement techniques”, *Nucl. Eng. Des.*, **337**, pp.205-220 (2018).
22. T. Glantz, T. Taurines, O. De Luze, S. Belon, G. Guillard, and F. Jacq, “DRACCAR: A multi-physics code for computational analysis of multi-rod ballooning, coolability and fuel relocation during LOCA transients Part one: General modeling description”, *Nucl. Eng. Des.*, **339**, pp. 269-285 (2018).
23. P. Chatelard, S. Belon, L. Bosland, L. Carénini, O. Coindreau, F. Cousin, C. Marchetto, H. Nowack, L. Piar, and L. Chailan, “Main modelling features of the ASTEC V2.1 major version”, *Ann. Nucl. Energy*, **93**, pp. 83-93 (2016).